Inorganica Chimica Acta 507 (2020) 119583

Contents lists available at ScienceDirect

Inorganica Chimica Acta

journal homepage: www.elsevier.com/locate/ica

Research paper

Development of a colorimetric and fluorescent Cu^{2+} ion probe based on 2′-hydroxy-2,4-diaminoazobenzene and its application in real water sample and living cells

Ren Hong*, Wu Ping, Li Fei, Yu Shihua, Jin Li, Lou Dawei

School of Chemistry and Pharmaceutical Engineering, Jilin Institute of Chemical Technology, Jilin City 132022, PR China

ARTICLE INFO

Keywords:
Colorimetric
Off–on fluorescence probe
Ortho-amino azobenzene
Cu^{2+} ion
1,2,3-Triazole

ABSTRACT

2′-Hydroxy-2,4-diaminoazobenzene (**L1-OH**), a fluorescence probe bearing ortho hydroxyl and amino group for the detection of Cu^{2+} ion was synthesized through diazo coupling reaction. The visible color change of **L1-OH** from yellow to pink was attributed to the coordination with Cu^{2+}. The 1:1 binding mode of **L1-OH** with Cu^{2+} was confirmed by UV titration, Job-plot method and ethylene diamine tetraacetic acid (EDTA) chelation experiment. Meanwhile, the non-emissive **L1-OH** (Fluorescence quantum yield, $\Phi = 0.003$) has transformed into fluorescent benzotriazole derivative 2-(2-hydroxy-phenyl)–2H-5-aminobenzo[d][1–3]triazole (**L1-OH-BTA**) ($\Phi = 0.27$) by adding Cu^{2+}, which was supported by the HPLC spectra and DFT calculations. **L1-OH** was applied for quantitative detection of Cu^{2+} with good linear relationship between UV absorbance, fluorescence intensity and Cu^{2+} concentration, and exhibited high selectivity toward Cu^{2+} over other metal ions (Na^+, K^+, Ca^{2+}, Ag^+, Pb^{2+}, Zn^{2+}, Mn^{2+}, Mg^{2+}, Ni^{2+}, Fe^{2+}, Fe^{3+}, Co^{2+}, Cd^{2+} and Al^{3+}). Furthermore, the test paper dyed by **L1-OH** shown colorimetric detection soaking in practical water sample with Cu^{2+} ion ($\geq 10\,\mu M$). The **L1-OH** could also be used as a fluorescent probe for monitoring Cu^{2+} ion in living HepG2 cells.

1. Introduction

The probers bind to the analyte selectively, accompanied by change in one or more properties of the system, such as fluorescence, color, or redox potential. For the last 20 years, the development of chemical probes for Cu^{2+} ions with various of chemical structures and recognition mechanisms has considerable attention due to their application in biological, chemical, medical and environmental process [1]. The series of small organic molecules for Cu^{2+} ion detecting have been reported, containing rhodamine [2–5], coumarin [6,7], boron dipyrromethene [8,9], fluorescein [10], 8-hydroxyquinoline [11], and Schiff base derivatives [12–14] and so on. From the point of reaction mechanism, the probes generally fall into two classes: “on–off”, “off–on”. For the inherent paramagnetic nature of Cu^{2+}, the “on–off” fluorescent probe was more common than the “off–on” probes. But the “off–on” probes can interact with Cu^{2+} ions to afford the enhancement of fluorescence intensity, which can avoid offering false positive results of fluorescence quenching in some particular environment. In brief, the merits of the “off–on” chemosensor for Cu^{2+} ions make them more attractive than the “on–off” probe [15].

Meanwhile, azo compounds have become as signaling unit in fluorescence probes expanding from the traditional dyes industry. The ortho amino azobenzene, a subgroup of azobenzene, which can detect Cu^{2+} ion as “turn-on” fluorescence probe due to the Cu^{2+}-catalyzed oxidation reaction [16–22]. In the presence of Cu^{2+} ions, the ortho amino azobenzene can transform into 1,2,3-triazole ring, which lead to strong fluorescent emission. The disadvantage of paramagnetic nature has been overcome and inner oxidation ability of Cu^{2+} ion has been exploited. Moreover, the interaction of azobenzene and its derivatives with Cu^{2+} ions is often exhibit color changes, which is easy to distinguish by naked eye for colorimetric detection [23–25]. Very recently, our research group have successfully reported a visual colorimetric and fluorescence turn-on probe, 2,2′- diaminoazobenzene [16]. The 2,2′-diaminoazobenzene was capable of recognizing Cu^{2+} over other metal ions, accompanied by a visible color change from yellow to light-purple and a significant fluorescence enhancement through cyclization of *ortho*-amino azobenzene. Both the coordination and catalytic oxidation reaction can be observed within the interaction of probe to Cu^{2+} ions. As literatures, the *ortho*-amino azobenzene related compounds severed as chemosensors can recognize Cu^{2+} through irreversible oxidation reactions and reversible coordination process [21,22]. The further research based on *ortho*-amino azobenzene derivatives is worth of

* Corresponding author.
E-mail address: renhong_jl@163.com (R. Hong).

https://doi.org/10.1016/j.ica.2020.119583
Received 30 September 2019; Received in revised form 12 January 2020; Accepted 4 March 2020
Available online 07 March 2020

studying, for the flexible mood to detect Cu^{2+} ion and practical requirements for Cu^{2+} ion detection.

As the third most abundant transition metal ion only less than zinc and iron in the human body, copper plays an essential role in various biological processes. Living cells must maintain moderate concentration of copper ions to keep the normal functioning of enzymes and intracellular metabolic balance. The deficiency and excess of Cu^{2+} mainly results in severe diseases, such as myelodysplasia, anemia, leukopenia (low white blood cell count), neutropenia and Wilson's disease, Alzheimer's disease, Parkinson's disease, etc. Cu^{2+} is also a significant environmental pollutant due to its extensively applications in industry, agriculture, and human daily life [26,27]. The ideal fluorescent probes for Cu^{2+} ion should possess the merits of high sensitivity and specificity, low cost, simple operation, good reproducibility and non-destruction. Application of small organic molecules as chemosensor for transition and heavy metal ions have drawn continuous interest, but the poor water solubility and toxicity is an important issue that must be solved, they are still limited in practical applications to some extent [13,28-33]. To further study for fluorescent probes, the continuation of our previous work based on the *ortho*-amino azobenzene derivatives, we report in this full account the design, synthesis, and metal-ion sensing behavior of a new compound, 2′-hydroxy-2,4-diaminoazobenzene (**L1-OH**). The reaction mechanism of probe **L1-OH** and the effect of –OH group on recognition were investigated systematically by instrumental analysis and chemical methods. The practical application of **L1-OH** on real water sample and HepG2 cell has been reported to pave path for more reliable and sophisticated chemosensors based on ortho amino azobenzene.

2. Results and discussion

2.1. Colorimetric study of L1-OH to Cu^{2+} ion

The UV absorbance spectrum of **L1-OH** was determined in EtOH solution at a concentration in range of 6.67 ~ 33.33 μM, revealing the strong absorption peak at 465 nm, a linear relationship was observed between the absorption intensity and concentration of **L1-OH** with molar absorption coefficient $\varepsilon = 2.403 \times 10^4\,L{\cdot}mol^{-1}{\cdot}cm^{-1}$ (Fig S1). The relative big value of ε can make colorimetric response between **L1-OH** and Cu^{2+} more sensitive. Initially, the sensing ability of **L1-OH** toward various metal cations (Na^+, K^+, Ca^{2+}, Ag^+, Pb^{2+}, Zn^{2+}, Mn^{2+}, Mg^{2+}, Al^{3+}, Ni^{2+}, Fe^{2+}, Fe^{3+}, Co^{2+}, Cd^{2+}, and Cu^{2+}) has been investigated qualitatively by visual examination of the cation-induced color changes of the receptor. As shown in Fig. 1, upon the addition of 1.0 equiv. of Cu^{2+} ions to the solution of **L1-OH** (16.7 μM), the obvious color change was observed instantly from yellow to light pink. By contrast, the addition of other surveyed metal ions failed to cause any vivid color change, which reflects the capability of **L1-OH** to response Cu^{2+} ion selectively. To provide fundamental insights into the suitability of **L1-OH**, the Cu^{2+} ion recognition behavior of the sensor was explored using UV–Vis spectroscopy upon the addition of various concentrations of cations to ligand solution. The UV–Vis spectrum of the free ligand exhibited an intense band centered at 465 nm which is attributed to the π-π* transition. Upon the addition of various metal ions, only Cu^{2+} was able to have a profound effect on the electronic spectrum of **L1-OH**. Addition of aqueous solution of Cu^{2+} ion to the **L1-OH** solution led to the emergence of a new band with absorption maxima at 505 nm with a simultaneous decrease in the absorbance at 465 nm. However, no such apparent spectral changes were induced by the addition of other metal ions. To further assess the binding characteristics of **L1-OH**, the UV–Vis spectroscopic titration of **L1-OH** (16.7 μM) were performed with Cu^{2+} ion. With increasing Cu^{2+} concentration, the isosbestic points at about 482 nm can be observed explained by the form of "Cu^{2+} + **L1-OH**" complex. A plot of absorbance at 505 nm of **L1** vs Cu^{2+} concentration (8.33 ~ 16.7 μM) showed a linear relation, hence the quantitative detection of Cu^{2+} via UV–Vis absorption is possible. The limit of detection (LOD) in UV–Vis is estimated to 8.33 μM for Cu^{2+} ion, which is much lower than the World Health Organization (WHO) recommended level (below 30 μM) for safe drinking (Fig. 2a). The binding constant of the complex was determined from the intensity data according to Benesi–Hildebrand equation [24]. Accordingly, the measured absorbance $1/[A\text{-}A_0]$ varied as a function of $1/[Cu^{2+}]$ in a linear relationship, supporting 1:1 stoichiometry between **L1-OH** and Cu^{2+} with binding constant of 4.157×10^4 (Fig. 2b). The pattern of absorption spectra remained unchanged when more than 1.0 eq of Cu^{2+} was added, corroborated with the formation of a 1:1 (M:L) complex, and the same conclusion was obtained using the continuous-variation plot (Job's plot) (Fig. 3a) [34-36]. To further prove the coordination ability of **L1-OH** to Cu^{2+}, the addition of EDTA to **L1-OH** and Cu^{2+} system showed that the process of titrating **L1-OH** with EDTA was reversible at 5–6 times, reflecting the chelation Cu^{2+} with **L1-OH** and repeatability of the **L1-OH** as colorimetric sensor (Fig. 3b).

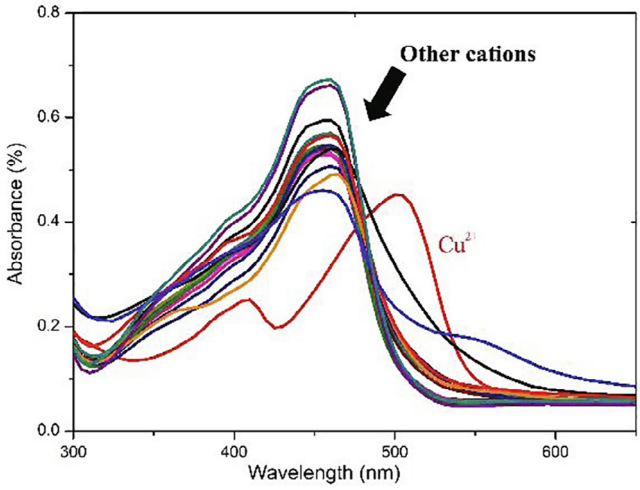

Fig. 1. UV absorption spectra of **L1-OH** (16.7 μM) in the presence of 1.0 equiv. of different cations (Na^+, K^+, Ca^{2+}, Ag^+, Pb^{2+}, Zn^{2+}, Mn^{2+}, Mg^{2+}, Al^{3+}, Ni^{2+}, Fe^{2+}, Fe^{3+}, Co^{2+}, Cd^{2+} and Cu^{2+}).

Most of the probes are performed only in the solution phase and hence this restricts their practical applications. Therefore, to evaluate the potential use of the sensor **L1-OH** to determine Cu^{2+} ions in real water samples, **L1-OH** loaded test paper was prepared. The target test papers were simply produced by immersing filter papers into EtOH solution of **L1-OH** (5×10^{-4} M) and then drying in air for 20 min. To investigate whether **L1-OH** could be applicative to real samples under laboratory condition, the experiments were performed in Quanyangquan drinking mineral water samples (Major Components: H_2SiO_3 25.0–35.0 mg/L, K^+ 0.8–3.0 mg/L, Na^+ 1.7–5.8 mg/L, Ca^{2+} 3.1–5.9 mg/L, Mg^{2+} 1.6–7.1 mg/L), which is sourced from Changbai Mountain 5A Natural Scenic Reserve in Jilin Province, China. Without any spectroscopic instrumentation, the test paper dyed with **L1-OH** was soaked in aqueous solution to be measured (Adding a certain range concentration of copper ion in advance: ≥10 μM), the marked color change from yellow to light pink was observed immediately (Fig. 4). The rapid and obvious color change of the test paper reflects the practical application of **L1-OH** for water quality monitoring. To evaluate the selectivity of **L1-OH** for Cu^{2+} (5×10^{-4} M), a variety of metal ions with same concentration including Na^+, K^+, Ca^{2+}, Ag^+, Pb^{2+}, Zn^{2+}, Mn^{2+}, Mg^{2+}, Ni^{2+}, Fe^{2+}, Fe^{3+}, Co^{2+}, Cd^{2+} and Al^{3+} were examined under the same condition as Cu^{2+}, the fast and sharp color change of the test paper can also be seen, indicating the sensor is promising for the analysis of environmental samples. It is noted that the test paper can be regenerated by immersing in EDTA (5×10^{-3} M) solution for around 5 min. The pH scope of application is 2.0 ~ 12.0, which is determined by adding various pH buffer solution to mixture to

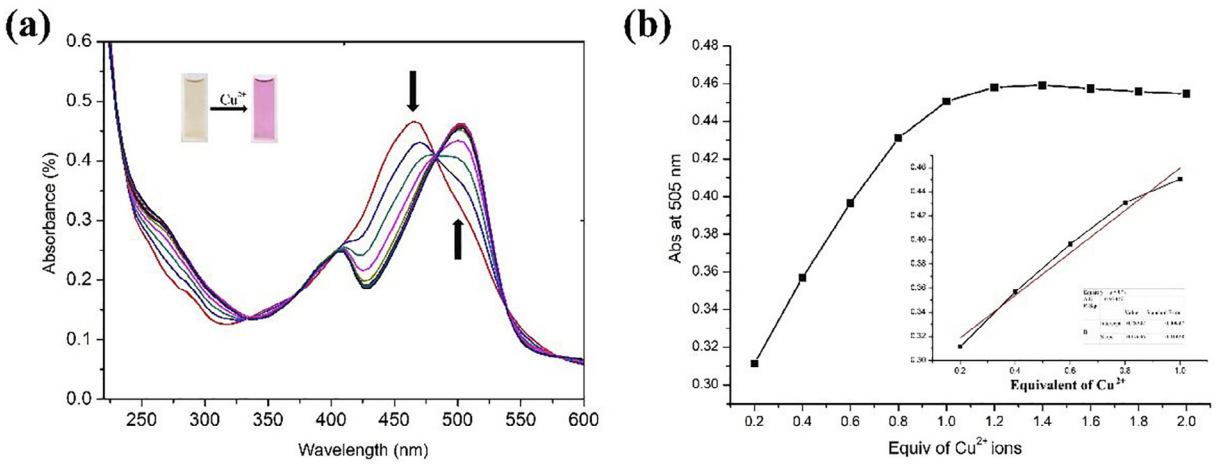

Fig. 2. (a) UV spectrophotometric titrations of **L1-OH** (16.7 μM) with various numbers of equivalents of Cu(II) ion in EtOH solution. (Insert: colour change of **L1-OH** and with Cu^{2+}); (b) The linear relationship of Abs vs different concentrations of the Cu^{2+} ion at 505 nm.

be measured. The fast on-site detection of copper ion based on **L1-OH** has been demonstrated using easy-to-prepare test papers.

2.2. Fluorescence spectral response of L1-OH to Cu^{2+} ion

In the fluorescence titration experiment, the **L1-OH** at a concentration of 1.0 μM was subjected to excitation at 365 nm and was monitored after each stepwise addition of Cu^{2+} ions to the solution. A gradual enhancement of the fluorescence intensity was observed at 477 nm with the equiv of Cu^{2+} ion to **L1-OH** from 0.25 to 5.0, and the mixture of **L1-OH** and Cu^{2+} ion showed fluorescently blue-green, which has distinction of **L1-OH** solution. A linear relationship between the fluorescence intensity of **L1-OH** and Cu^{2+} concentration can be seen in a range of 0.25 ~ 3 μM and the limit of detection (LOD) of **L1-OH** for Cu^{2+} was calculated to be 0.208 μM by the equation LOD = (3.3 σ/*k*). In which σ is the standard deviation of the y-intercepts of the regression lines, and *k* is the slope of the calibration graph (Fig. 5) [37].

The selectivity of the **L1-OH** (1.0 μM) toward various metal ions was investigated by monitoring the fluorescence intensity change after adding with a number of metal ions with concentration of 1.0 μM, for example Na^+, K^+, Ca^{2+}, Ag^+, Pb^{2+}, Zn^{2+}, Mn^{2+}, Mg^{2+}, Ni^{2+}, Fe^{2+}, Fe^{3+}, Co^{2+}, $Cd^{2+}$and Al^{3+}. It was noted that only addition of Cu^{2+} (1.0 μM) resulted in a dramatic fluorescence enhancement of the solution of **L1-OH**, while other metal ions resulted in no significant response to the fluorescence spectra. To gain more insight into the selectivity toward Cu^{2+}, a competition experiment was carried out by the addition of Cu^{2+} (1.0 μM) in the presence of other species with concentration at 20 μM. Interestingly, the metal ions Na^+, K^+, Ca^{2+}, Ag^+, Pb^{2+}, Zn^{2+}, Mn^{2+}, Mg^{2+}, Ni^{2+}, Fe^{2+}, Fe^{3+}, Co^{2+}, Cd^{2+} and Al^{3+} did not interfere with the Cu^{2+} enhanced fluorescence (Fig. 6).

Since the fluorescence properties of **L1-OH** could be influenced by pH value, the response property of **L1-OH** were discussed by adding a certain volume buffered solutions with various pH values into the EtOH solution of **L1-OH** (pH range from 2.0 to 12.0, the step-size was 1.0 pH unit). Over a wide pH range of 3 ~ 10, the fluorescence band at 477 nm increased suddenly and **L1-OH** is insensitive to pH, suggesting the sensor could be applied successfully for Cu^{2+} detection under physiological conditions. In addition, we evaluated the time course of fluorescent response of probe **L1-OH** (1 μM) to Cu^{2+} (1 mM) in 3 mL EtOH. The reaction of **L1-OH** and Cu^{2+} went rapidly in the first five minutes, which can be completed within 10 min. Therefore, **L1-OH** absolutely could be applied in real-time determination of Cu^{2+} in environmental and biological conditions. The series of solutions have been designed to study the influence of ethanol: water. The strongest fluorescence intensity can be observed in pure ethanol solution, and the fluorescence intensity has gradually become weak along with the increasing of water volume proportion (Fig S2).

To further demonstrate its biological applications, we explored fluorescence bioimaging of **L1-OH** to monitor Cu^{2+} in HepG2 cells. HepG2 cells were cultured in modified Eagle's medium (MEM)

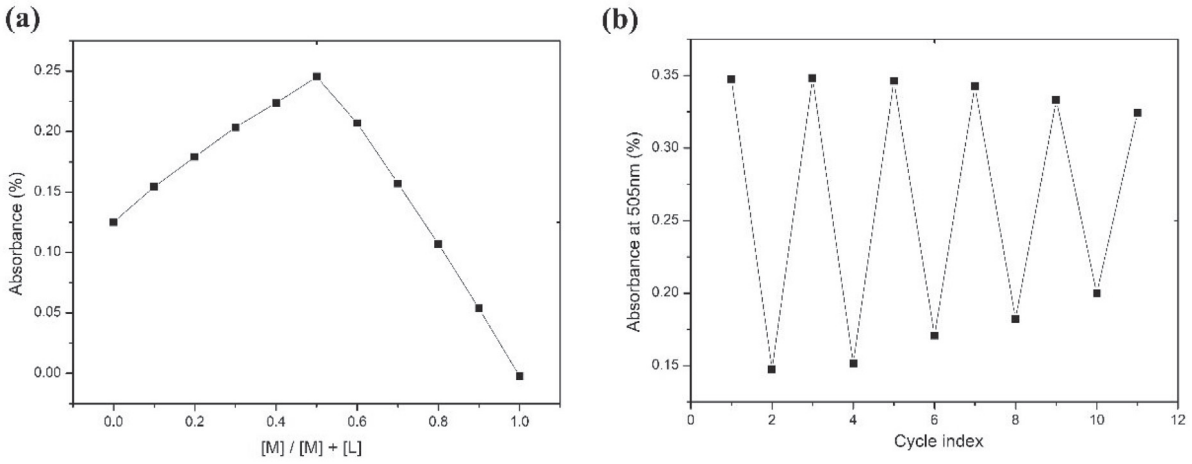

Fig. 3. (a) The UV titration profiles for Job's method to confirm the 1:1 equivalent ratio of the M:L binding stoichiometry of the complex in EtOH under 505 nm; (b) UV adsorption switching cycles of **L1-OH** (16.7 μM) controlled by alternating addition of EDTA and Cu^{2+} in EtOH solution.

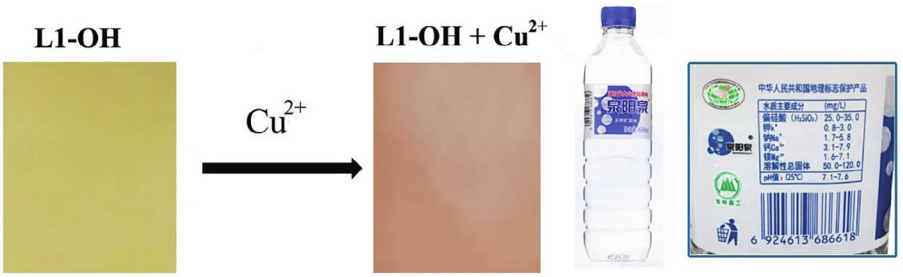

Fig. 4. Yellow paper treated with **L1-OH** is turn into pink paper at the effect of Cu^{2+} ion and the bottle of Quanyangquan drinking mineral water. (For interpretation of the references to color in this figure legend, the reader is referred to the web version of this article.) (For interpretation of the references to color in this figure legend, the reader is referred to the web version of this article.)

supplemented with 10% fetal bovine serum (FBS) under humidified atmosphere of CO_2/ air (5: 95%) at 37 °C. Prior to imaging experiments, the cells (3×10^5/well) were seeded in a 12-well plate. After 24 h, the cells were washed with PBS buffer (pH = 7.4). HepG2 cells were first cultured with **L1-OH** (40 μM, aqueous solution) for 30 min in 0.01 M PBS buffer. After that, cells were washed repeated with PBS for three times, and then with $CuSO_4$ (0.5 mM) for 1 h. As shown in Fig. 7, strong fluorescence can be observed after HepG2 cells pretreated by **L1-OH**. In contract, cell display no fluorescence in the presence of Cu^{2+}, and cells treated with only **L1-OH** remained non-emissive. These experimental results manifested that **L1-OH** possessed good cell permeable as well as could be used for the detection of Cu^{2+} in living cell. Moreover, the CCK8 method was used to detect the effect of probe **L1-OH** on cell viability. The most of HepG2 cells are alive with high OD value (93.0%) accompanied by the 40 μM **L1-OH** incubated in cells for 24 h.

2.3. Proposed mechanism

Upon being exposed to Cu^{2+}, N=N isomerization of **L1-OH** was suppressed by selective catalytic cyclization to triazole which are confirmed by the same type of probes (Fig. 8a) [16-21]. In order to confirm the recognition mechanism of **L1-OH**, the benzotriazole product **(**2-(2-hydroxy-phenyl)–2H-5-aminobenzo[d][1–3]triazole, **L1-OH-BTA)** was gained directly and defined clearly by 1H NMR, 13C NMR, Mass and IR spectra, which has shown the emission peak at 478 nm (Fig. 8b). The position of the peak is corresponding to the fluorescence spectra of "**L1-OH** + Cu^{2+}", which can afford demonstration mechanism of Cu^{2+}-catalyzed oxidative cyclization to fluorescence **L1-OH-BTA**. The fluorescence quantum yields Φ of **L1-OH** and **L1-OH-BTA** have been determined by quinine sulfate as a reference (**L1-OH**, Φ = 0.003; **L1-OH-BTA,** Φ = 0.27). The addition of excess EDTA to the complex solution of **L1-OH**-Cu^{2+} did not disturb the fluorescence emission, suggesting the irreversible catalysis process rather than chelation in fluorescence spectra (Fig. 8c) [26,34]. Moreover, the product of the reaction between **L1-OH** and Cu^{2+} was analyzed by High performance liquid chromatography (HPLC). Under the pretreatment and chromatographic conditions, the retention time of **L1-OH** and **L1-OH-BTA** was 5.94 and 7.68 min respectively, and most of **L1-OH** has been transformed into **L1-OH-BTA** (Fig. 8d).

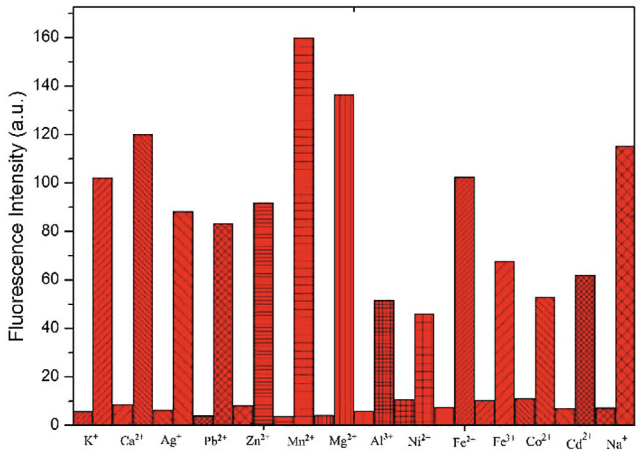

Fig. 6. Fluorescence intensity changes of the **L1-OH** (1.0 μM) to Cu^{2+} (1.0 μM) in the presence of various teat cations (20 equiv) in EtOH solution at λ = 477 nm (λ_{exc} = 360 nm) (Lower: Competition ion; Higher: Competition ion + Cu^{2+} ion).

2.4. Density functional theory (DFT) calculations

For gain more information on the nature of the probe **L1-OH** with Cu^{2+}, energy-optimized structures of **L1-OH** and its corresponding benzotriazole product **L1-OH-BTA** were studied by density functional theory (DFT) calculations at the B3LYP level using 6-31G basis set

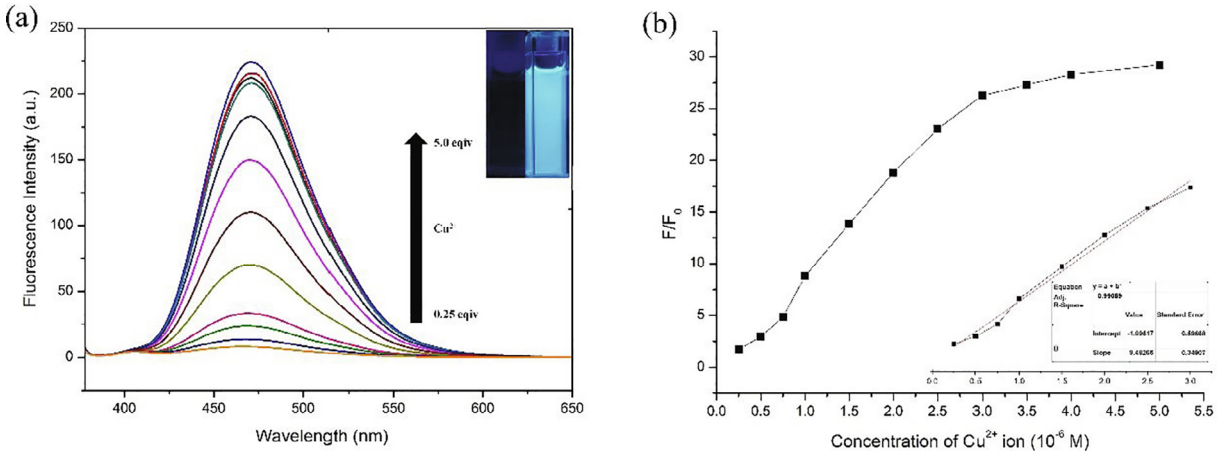

Fig. 5. (a) Fluorescence spectra of **L1-OH**(1.0 μM) with addition different concentrations of Cu^{2+} (0.0 ~ 5.0 equiv) in EtOH solution. Insert: color change of **L1** and with Cu^{2+} under UV lamp. (b) The linear relationship of relative fluorescence intensity vs different concentrations of the Cu^{2+} ion at 476 nm.

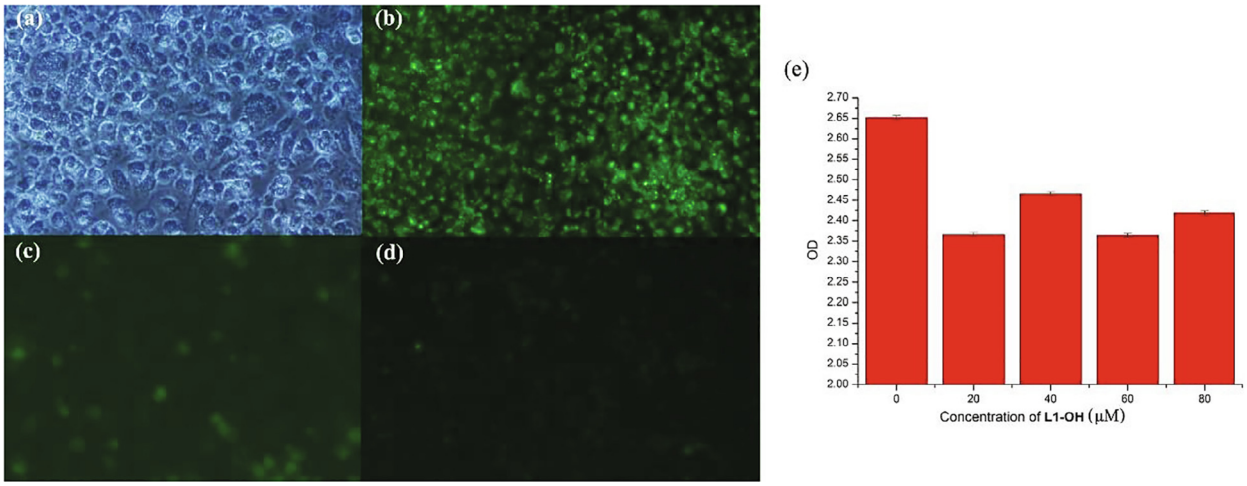

Fig. 7. Fluorescence imaging of HepG2 cells. (a) Bright-field image of HepG2 cells preloaded with probe **L1-OH** (5 μM) in PBS (0.01 M, pH 7.4) for 30 min at 37 °C. (b) Fluorescence image in green channel of HepG2 cells preloaded with Cu^{2+} (5 mM) for additional 1 h. (c) Fluorescence image in green channel of HepG2 cells treated only with L-OH (40 μM) for 30 min. (d) Fluorescence image in green channel of HepG2 cells treated only with Cu^{2+} (5 mM) for 1 h. (e) The effects of different concentrations of **L1-OH** on the HepG2 cells by cck8 method for 24 h. (For interpretation of the references to color in this figure legend, the reader is referred to the web version of this article.) (For interpretation of the references to color in this figure legend, the reader is referred to the web version of this article.)

through the Gaussian 09 program [38]. The electron distributions and orbital energies of the highest occupied molecular orbital (HOMO) and the lowest unoccupied molecular orbital (LUMO) of probe **L1-OH** and **L1-OH-BTA** are exhibited in Fig. 9. From the point of energy, the energy gaps between the HOMO and LUMO of the **L1-OH** and **L1-OH-BTA** were calculated to be 1.562 eV, 3.578 eV, respectively. The results indicated that benzotriazole product **L1-OH-BTA** increased the HOMO–LUMO energy gap of the molecular. The **L1-OH** can transfer easily between different energy states for relative lower energy gap, which has consumed energy and lead to the non-fluorescent phenomenon. While **L1-OH** can transform to **L1-OH-BTA** in the presence of Cu^{2+}, the high density electron cloud on benzotriazole ring can be assigned to the redistribution of π electrons, resulting in the increasing of emission intensity.

2.5. Comparative discussion L1-OH to relative ortho-amino azobenzene probes

Compare with our previous work 2,2′-diaminoazobenzene (**L1**), we have introduced electron-donating –OH group onto a simple *ortho*-amino azobenzene (**L1-OH**), and the effect of –OH substituents on recognition Cu^{2+} ion displayed in many aspects. For UV spectra, the molar absorption coefficient ε of **L1** is equal to $1.35 \times 10^4\ L{\cdot}mol^{-1}{\cdot}cm^{-1}$, while the ε of **L1-OH** is $2.40 \times 10^4\ L{\cdot}mol^{-1}{\cdot}cm^{-1}$. For the absorption (A) should fall within 0.2–0.7 range to ensure the accuracy of measurement, larger ε corresponds to lower detection limit (LOD) under Lambert-Beer law. In UV spectra, the LOD of **L1** and **L1-OH** is 16.7 μM and 8.33 μM, respectively. The test paper based on **L1** is prepared with the similar method of **L1-OH**, the applicable pH range is 4.0 ~ 9.2 for **L1** (Fig S3), which is narrow than that (2.0–12.0) of **L1-OH**. As for fluorescence spectra, the

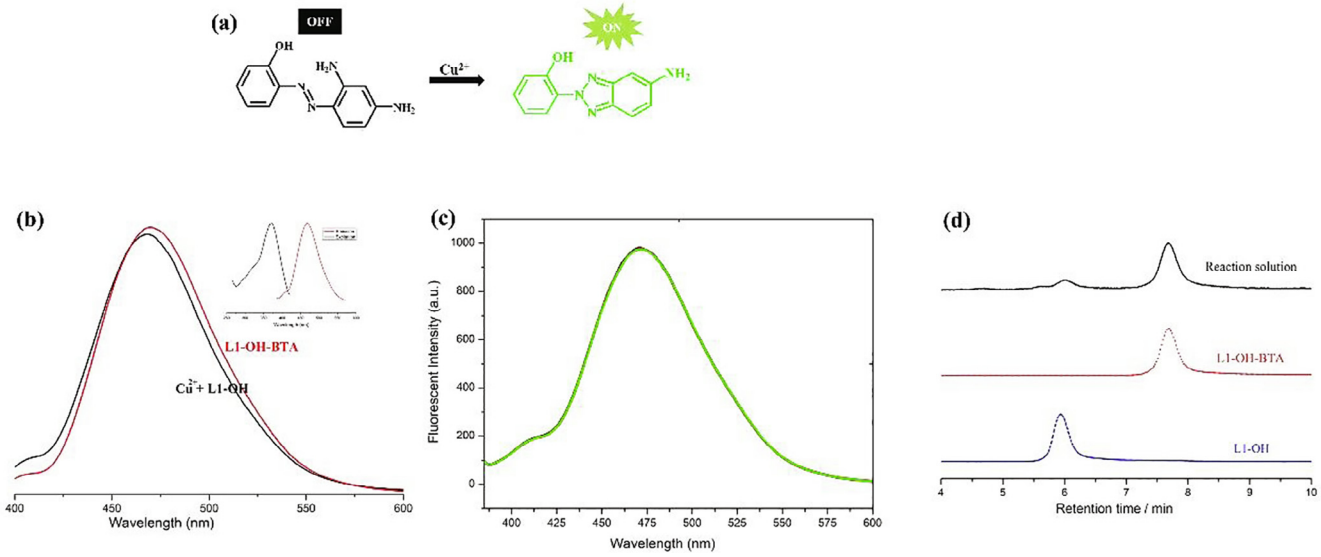

Fig. 8. (a) Proposed mechanism of the probe **L1-OH** to Cu^{2+} ion. (b) Black solid line: fluorescence spectra of **L1** with addition Cu^{2+} in EtOH solution; Red dotted line: the curve of benzotriazoles product of **L1**.Insert: The emission and excitation fluorescence spectra of **L1-OH-BTA**. (c) The fluorescence emission spectra of solution of "**L1-OH** + Cu^{2+}" adding with EDTA with same concentration of **L1-OH**. Black line: **L1-OH** + Cu^{2+}; green and red lines: **L1-OH** + Cu^{2+} + EDTA. (d) Chromatogram of **L1-OH**, **L1-OH-BTA**, and reaction solution. (For interpretation of the references to color in this figure legend, the reader is referred to the web version of this article.) (For interpretation of the references to color in this figure legend, the reader is referred to the web version of this article.)

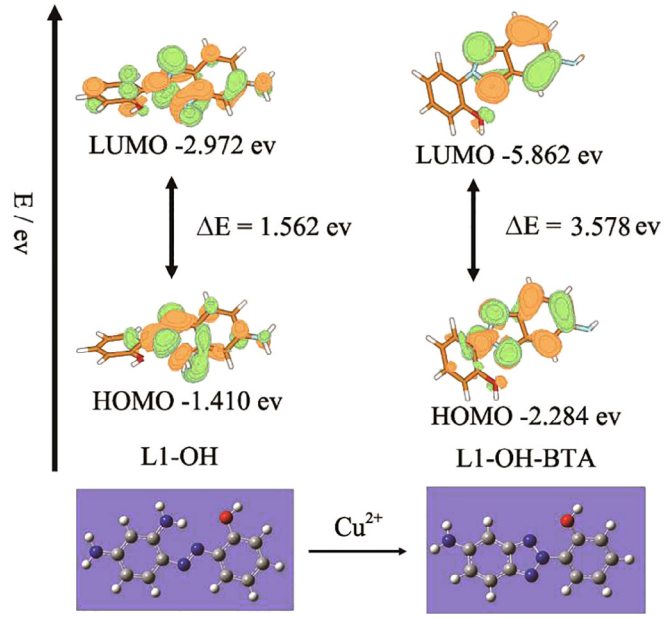

Fig. 9. Electron distribution and energy diagram of HOMO and LUMO orbitals for **L1-OH**, **L1-OH-BTA** calculated at the DFT level.

LOD of Cu^{2+} ion for **L1-OH** is 0.208 μM, which is superior to **L1** (0.648 μM). For **L1-OH**, the detection of Cu^{2+} in EtOH solution could be accomplished within 10 min at room temperature. The interaction of **L1** and Cu^{2+} finished within 20 min, which takes twice as long of **L1-OH**. In brief, the **L1-OH** is superior to **L1** as visual colorimetric and fluorescence turn-on probe.

Generally, the family of o-amino benzobenzene chemosensor themselves are non-fluorescent, while a fluorophore can be released via the Cu^{2+}-promote oxidative cyclization of the chemsensor. A brief summary on the o-amino benzobenzene chemsensor are given in Table 1. Compared with these reported probes, the solvent EtOH for our probes (**L1** and **L1-OH**) had a relative lower toxicity and the LOD is capable to monitor the trace Cu^{2+} to achieve drinking standard of WHO. One of outstanding advantage of **L1-OH** is that it is applicable for the determination of Cu^{2+} in living cells at pH = 7.4. Moreover, the test paper based on the visual colorimetric properties of **L1-OH** can be used for practical water monitoring, which expand the scope in analytical application.

3. Conclusions

We have successfully devised a new chemsensor **L1-OH** (2′-hydroxy-2,4-diaminoazobenzene) for Cu^{2+} ion recognition based on coordinate and catalytic reaction. The **L1-OH** is efficiently recognize Cu^{2+} over other metal ions (Na^{+}, K^{+}, Ca^{2+}, Ag^{+}, Pb^{2+}, Zn^{2+}, Mn^{2+}, Mg^{2+}, Ni^{2+}, Fe^{2+}, Fe^{3+}, Co^{2+}, Cd^{2+} and Al^{3+}), and rapid colorimetric and fluorescence turn-on detection can be gained, showing a visible color change form yellow to pink and a significant fluorescence enhancement, respectively. The titration reaction, HPLC, and relative chemical studies are introduced to give insight of coordination and oxidative cyclization process. The successful preparation of test paper and HepG2 cell imaging based on **L1-OH** has become as a promising platform for a variety of sensing applications in environmental, biological and relative areas.

4. Experimental section

4.1. Materials and methods

All the chemicals were commercially available at analytic grade and

Table 1
The comparison of **L1-OH** with other reported probes based on *ortho*-amino azobenzene in the literature.

Methods	Mechanism types	Liner range/μ mol·L^{-1}	LOD/μ mol·L^{-1}	Solvent	Optimal pH range	λem (nm)	Application
This paper	Oxidative cyclization + Coordination	0.25–3	0.208	EtOH	3–10	477	HepG2 cells; Mineral water sample
		8.33–16.7	8.33 (UV)				
[16]		greater than 116	0.648	EtOH	–	475	–
		.7–83.3	16.7 (UV)				
[17]	Oxidative cyclization	0.02–5	0.02	PBS buffer/CH_3CN (9:1, v/v; pH = 7.4)	3–10	510	–
[18]		–	~100	DMSO/HEPES (v/v, 0.2: 9.8; pH = 7.2)	–	484	–
[19]		–	~300	CH_3CN	–	455	–
[20]		0–40 (UV)	0.0144	MeOH/HEPES solution (8:2, v/v; pH = 7)	–	490	MCF-7 cells
		0–20					
[21]	Compound **8**	10–60	10	H_2O (pH = 7.0; HEPES, 50 mM)	6.0–8.0	530	–
[22]	Complexation mood (BDA: Cu^{2+} = 2:1)	0–5	0.12	CH_3CN/Tris-HCl buffer (v:v = 2:8, pH = 7.20)	–	407	drinking water samples + photo print

used as received. Fresh double distilled water was used throughout the experiment. NMR spectra were recorded on a Bruker-400 spectrometer with chemical shifts reported as parts per million (ppm; in DMSO-d_6, TMS as internal standard). IR spectra were collected on a Nicolet Impact 410 spectrometer between 400 and 4000 cm^{-1}, using the KBr pellet method. Mass spectra were recorded on a Thermo mass spectrometer. UV–vis spectra were obtained with a Cary 60 spectrophotometer of Agilent Technologies. The fluorescence data were determined on a Perkin-Elmer LS 45 luminescence spectrometer. For all luminescence measurement, excitation and emission slit widths of 10 nm were used. The wave number of excited light for UV lamp is 365 nm. The cell experiment were carried out with Nikon eclipse T*i* microscope. High performance liquid chromatography (HPLC) analysis was carried out on a Shimadzu LC-20AB system (Kyoto, Japan) equipped with a CTO-10A Scolumn oven and a SPD-M20A detector. The chromatographic separation of analysts was taken on a VP-ODS C18 column (4.6 mm × 250 mm, 5 μm). The mobile phase used was methanol/water (70: 30). Its flow rate was 1.0 mL/min and the detection wavelength was detected at 280 and 311 nm for **L1-OH** and **L1-OH-BTA** respectively. The injection volume was 20 μL and both the concentrations of **L1-OH** and **L1-OH-BTA** are maintained at100 mg/L.

4.2. Preparation of L1-OH and L1-OH-BTA

Preparation of **L1-OH**: the target compound was synthesized from o-aminophenol and m-phenylenediamine as raw materials by diazo coupling reaction (Fig S4). In detail, 0.7 g o-aminophenol and 0.75 mL concentrated hydrochloric acid were mixed in a small beaker, then 3.25 mL ethanol were added and the mixture are placed in ice water. In addition, 0.7 g m-phenylenediamine solid was added to 4.0 mL water, dissolved and cooled in ice water. The solution of m-phenylenediamine was slowly added to o-aminophenol solution, and stirred for 30 min in ice-water bath. Sodium nitrite 0.4 g was dissolved in 1.0 mL of water, then slowly added to the above mixture, stirring for about 10 min. The Na_2CO_3 solution was used to adjust the pH of the reaction mixture at about 8.0, at which time the solid precipitated. Finally, the red-brown products was obtained and weighed through filtration.

L1-OH was fully characterized by ^{1}H NMR, ^{13}C NMR and IR spectra (Fig S5). ^{1}H NMR (400 MHz, DMSO-d_6) of **L1-OH**: δ 11.67 (s, 1H), 7.60 (dd, J = 8.3, 1.7 Hz, 1H), 7.31 (t, J = 9.9 Hz, 3H), 7.15–7.08 (m, 1H), 6.90 (ddd, J = 8.1, 6.6, 1.3 Hz, 2H), 6.05 (dd, J = 8.8, 2.3 Hz, 1H), 5.99 (s, 2H), 5.89 (d, J = 2.3 Hz, 1H). ^{13}C NMR (100 MHz, DMSO-d_6) of **L1-OH**: δ 153.48, 152.60, 146.54, 138.66, 131.77, 129.08, 128.15, 124.40, 119.86, 117.65, 106.48, 97.16. In the IR spectra of **L1-OH**, the two peaks at 3455 and 3362 cm^{-1} are attributed to the stretching vibrational mode of hydroxyl (–OH) and amino (–NH_2) groups. The vibration band around 1600 cm^{-1} can be assigned to the stretching vibrational mode of azo (N═N)groups.

Preparation of **L1-OH-BTA** (Benzotriazole products of **L1-OH**): The **L1-OH-BTA** was synthesized with **L1-OH** as raw material and Cu^{2+} as an oxidant. The ^{1}H NMR, ^{13}C NMR and IR spectra of **L1-OH-BTA** are described in Fig. S6. ^{1}H NMR (400 MHz, DMSO-d_6) of **L1-OH-BTA**: δ 10.89 (s, 1H), 8.02–7.86 (m, 1H), 7.73 (d, J = 9.1 Hz, 1H), 7.41–7.28 (m, 1H), 7.14 (dt, J = 14.3, 7.1 Hz, 1H), 7.09–6.98 (m, 2H), 6.73 (d, J = 1.4 Hz, 1H), 5.72 (s, 2H). ^{13}C NMR (100 MHz, DMSO-d6) of **L1-OH-BTA**: δ 149.94, 149.10, 145.62, 138.39, 130.29, 126.73, 123.06, 122.97, 120.26, 118.59, 118.47, 92.34. In the IR spectra of **L1-OH-BTA**, the new peak around 3000 cm^{-1} is corresponding to the formation of benzotriazole ring. MS (ES-API): calcd. for $C_{12}N_4OH_{11}$ $[M + H]^+$: 227.2; found 227.1.

4.3. General procedure for spectroscopy

Preparation of **L1-OH** solution for UV: To obtain C-A relationship, the **L1** solution at concentration of 5×10^{-4} mol·L^{-1} were added 40, 60, 80, 100, 120, 140, 160, 180, 200 μL per time in alcohol solution to maintain the whole volume as 3.0 mL. UV spectral titration of azo compound solution with various metal salts: Initial solution is composed of 0.1 mL 5.0×10^{-4} mol·L^{-1} **L1-OH** in 2.9 mL alcohol solution. Then the above solution was gradually added by salt solution (5×10^{-4} mol·L^{-1}) by 20 μL per time. The formation of a 1:1 complex in solution can be achieved by mixing the Cu(II) salt and **L1-OH** solution with same concentration (16.7 μM), the volume is from 0 μL to 200 μL. UV absorption switching cycles of **L1-OH** (16.7 μM) controlled by alternating addition of EDTA and Cu^{2+} salt solution 10 μL per time with same concentration (5×10^{-3} mol·L^{-1}). Meanwhile, the fluorescence spectroscopy of **L1-OH** were recorded upon the addition of metal salts while keeping the azo concentration at 1.0 μM. The EDTA solution is added to the "**L1-OH** and Cu^{2+}" mixture, and the mole ratio of **L1-OH** to EDTA introduced is 1:2 and 1:4, separately. The concentration of reaction solution between "**L1-OH** and Cu^{2+}" used for HPLC is 16.7 μM for both Cu^{2+} and **L1-OH**, and the mixture showed strong fluorescence at 477 nm after 20 h.

Declaration of Competing Interest

The authors declare that they have no known competing financial interests or personal relationships that could have appeared to influence the work reported in this paper.

Acknowledgment

This work is supported by the Scientific Research Fund of Jilin Institute of Chemical Technology (No. 2019002) and the National Nature Science Foundation of China (No. 21375046, 21405058). Supporting Information Available.

Appendix A. Supplementary data

Supplementary data to this article can be found online at https://doi.org/10.1016/j.ica.2020.119583.

References

[1] D. Udhayakumari, S. Naha, S. Velmathi, Anal. Methods 9 (2017) 552–578.
[2] V. Dujols, F. Ford, A.W. Czarnik, J. Am. Chem. Soc. 119 (1997) 7386–7387.
[3] Z. Zhang, C.Q. Deng, H.H. Song, Inorg Chem Comm. 95 (2018) 56–60.
[4] K. Wechakorn, S. Prabpail, K. Suksen, P. Kanjanasirirat, Y. Pewkliang, S. Borwornpinyo, P. Kongsaeree, Luminescence 33 (2018) 64–70.
[5] L. Wang, D.D. Ye, W.X. Li, Y.Y. Liu, L.H. Li, W.L. Zhang, L. Ni, Spectrochimica Acta Part A: Molecular and Biomolecular Spectroscopy 183 (2017) 291–297.
[6] S.S. Wang, Z. Wang, Y. Yin, J.G. Luo, L.Y. Kong, Journal of Photochemistry and Photobiology A: Chemistry 333 (2017) 213–219.
[7] A.K. Mahapatra, S. Mondal, S.K. Manna, K. Maiti, R. Maji, M.R. Uddin, S. Mandal, D. Sarkar, T.K. Mondalc, D.K. Maiti, Dalton Trans. 44 (2015) 6490–6501.
[8] J.J. Shie, Y.C. Liu, Y.M. Lee, C. Lim, J.M. Fang, C.H. Wong, J. Am. Chem. Soc. 136 (2014) 9953–9961.
[9] W.J. Shi, J.Y. Liu, D.K.P. Ng, Chem. Asian J. 7 (2012) 196–200.
[10] F. Hou, J. Cheng, P. Xi, F. Chen, L. Huang, G. Xie, Y. Shi, H. Liu, D. Bai, Z. Zeng, Dalton. Trans. 41 (2012) 5799–5804.
[11] T. Branch, P. Girvan, M. Barahona, L. Ying, Angew. Chem. Int. Ed. Engl. 54 (2015) 1227–1230.
[12] F. Purtaş, K. Sayin, G. Ceyhan, M. Köse, M. Kurtoglu, Journal of Molecular Structure. 1137 (2017) 461–475.
[13] Y.L. Gao, C. Zhang, S.W. Peng, H.Y. Chen, Sensors and Actuators B 238 (2017) 455–461.
[14] G.J. Park, D.Y. Park, K.M. Park, Y. Kim, S.J. Kim, P.S. Chang, C. Kim, Tetrahedron 70 (2014) 7429–7438.
[15] S. Liu, Y.M. Wang, J. Han, J. Photochem. Photobiology C: Photochem. Rev. 32 (2017) 78–103.
[16] H. Ren, P. Wu, F. Li, J. Li, D.W. Lou, Inorg. Chim. Acta 487 (2019) 234–239.
[17] S. Cao, Q.Y. Jin, L. Geng, L.Y. Mu, S.L. Dong, New J. Chem. 40 (2016) 6264–6269.
[18] M. Gupta, A. Balamurugan, H. Lee, Sensors and Actuators B: Chemical. 211 (2015) 531–536.
[19] M. Gupta, H. Lee, Sensors and Actuators B: Chemical. 252 (2017) 977–982.
[20] Y.P. Wang, S.Z. Liu, H.B. Chen, Y.J. Liu, H.M. Li, Dyes and Pigments. 142 (2017) 293–299.
[21] J.Y. Jo, H.Y. Lee, W.J. Liu, A. Olasz, C.H. Chen, D. Lee, J. Am. Chem. Soc. 134 (2012) 16000–16007.
[22] Q.M. Wang, S.S. Wu, Y.Z. Tan, Y.L. Yan, L. Guo, X.H. Tang, Journal of

Photochemistry and Photobiology A: Chemistry. 357 (2018) 149–155.
[23] B. Kaur, N. Kaur, S. Kumar, Coordination Chemistry Reviews. 358 (2018) 13–69.
[24] J.M. Hong, H.Y. Kim, H. Park, S.K. Chang, Tetrahedron Letters 56 (2015) 6782–6785.
[25] K. Rezaeian, H. Khanmohammadi, V. Arab, Spectrochimica Acta Part A: Molecular and Biomolecular Spectroscopy 151 (2015) 848–853.
[26] B. Gu, L.Y. Huang, W. Su, X.L. Duan, H.T. Li, S.Z. Yao, Anal. Chim. Acta 954 (2017) 97–104.
[27] L.H. Wu, L.F. Han, Y.B. Ruan, Y.B. Jiang, Chin. J. Anal. Chem. 38 (2010) 121–124.
[28] A. Majumdar, C.S. Lim, H.M. Kim, K. Ghosh, ACS Omega 2 (2017) 8167–8176.
[29] M.A. Assiri, A.G. Al-Sehemi, M. Pannipara, Inorg, Chem. Comm. 99 (2019) 11–15.
[30] A. Reynal, J. Etxebarria, N. Nieto, S. Serres, E. Palomares, A. Vidal-Ferran, Eur. J. Inorg. Chem. (2010) 1360–1365.
[31] T. Sun, Q.F. Niu, T.D. Li, Z.R. Guo, H.X. Liu, Spectrochimica Acta Part A: Molecular and Biomolecular Spectroscopy 188 (2018) 411–417.
[32] T. Sun, Y. Li, Q.F. Niu, T.D. Li, Y. Liu, Spectrochimica Acta Part A: Molecular and Biomolecular Spectroscopy 195 (2018) 142–147.
[33] Q.C. Xu, Z.Y. Gu, G.W. Xing, Tetrahedron 15 (2017) 2123–2130.
[34] K. Chantalakana, N. Choengchan, P. Yingyuad, P. Thongyoo, Tetrahedron Letters. 57 (2016) 1146–1149.
[35] T. Wei, G. Liang, X. Chen, J. Qi, Q. Lin, Tetrahedron. 73 (2017) 2938–2942.
[36] A. Hens, P. Mondal, K.K. Rajak, Polyhedron. 85 (2015) 255–266.
[37] L. Jin, K.S. Zhang, F.T. Liu, Y. Wang, J.P. Zhang, Chin. J. Inorg. Chem. 4 (2018) 767–776.
[38] G.W. Frisch, H.B. Trucks, G.E. Schlegel, et al., Gaussian 09, Revision D.01, Gaussian Inc., Wallingford, CT, 2013.